RESEARCH　　　　　　　　　　　　　　　　　　　　　　　**Open Access**

CrossMark

Fractional difference co-array perspective for wideband signal DOA estimation

Jian-Yan Liu[2,1], Yi-Long Lu[2], Yan-Mei Zhang[1] and Wei-Jiang Wang[1*]

Abstract

In recent years, much attention has been focused on difference co-array perspective in DOA estimation field due to its ability to increase the degrees of freedom and to detect more sources than sensors. In this article, a fractional difference co-array perspective (FrDCA) is proposed by vectorizing structured second-order statistics matrices instead of conventional zero-lag covariance matrix. As a result, not only conventional virtual sensors but also the fractional ones can be utilized to further increase the degrees of freedom. In a sense, the proposed perspective can be viewed as an extended structured model to generate virtual sensors. Then, as a case study, four DOA estimation algorithms for wideband signal based on the FrDCA perspective are specifically presented. The fractional virtual sensors can be generated by dividing the wideband signal into many sub-band signals. Accordingly, the degree of freedom and the maximum number of resolvable sources are increased. The corresponding numerical simulation results validate the advantages and the effectiveness of the proposed perspective.

Keywords: Fractional difference co-array, Wideband signal DOA estimation, Enhancement of DOFs, Virtual sensor

1 Introduction

Direction of arrival (DOA) estimation is a critical problem in phased-array radar signal processing field [1]. Conventional DOA estimation methods (e.g., MUSIC [2] and ESPRIT [3]) were mainly based on the overdetermined uniform linear array (ULA) model (more sensors than sources). To detect more sources than sensors and maximize the spatial resolution, some non-uniform linear arrays (NLAs) were introduced into radar society, dating back to minimum redundancy arrays (MRAs) [4] or minimum hole arrays (MHAs) [5]. Many important advantages were validated in works [6–8] by forming augmented covariance matrices. Recently, due to the fact that second-order statistics (SOS) allowed us to gain more degrees of freedom (DOFs), several virtual co-array concepts based on SOS were proposed. Originally, the virtual array concept was used in multi-input multi-output (MIMO) radar system [9] through an active sensing scenario. Specifically, the MIMO radar could generate a group of sum co-arrays (SCA) that increase DOFs from $O(N + M)$

to $O(NM)$. A similar but not identical difference co-array (DCA) concept was proposed in [10], which could also generate virtual array and increase DOFs from $O(N)$ to $O(N^2)$ in a completely passive scenario by using a new NLA geometry called nested array. Following this notion, some new geometries were further developed such as co-prime array [11], generalized co-prime array [12], super nested array [13, 14], and dynamic array [15]. In [16, 17], the authors utilized multiple frequencies to fill the missing co-array elements, thereby enabling the co-prime array to effectively utilize all of the offered DOFs. In [18], the authors combined the DCA and the SCA and then proposed difference co-array of the sum co-array (DCSC), which offered a significant enhancement in the DOFs in active sensing scenario. In addition, a more general concept called compressive covariance sensing (CCS) was proposed in [19] by focusing on the reconstruction of the SOS matrix from sub-Nyquist samples.

The aforementioned DCA-based models were limited in narrowband signal case. Therefore, P. Pal, the founder of the DCA model, proposed an auto-focusing based method in [20] to extend the co-array concept into wideband signal case. However, the subspace information of many sub-bands has not been fully utilized due to the auto-focusing technique, and the maximum number of

*Correspondence: wangweijiang@bit.edu.cn
[1]School of Information and Electronics, Beijing Institute of Technology, 5 South Zhongguancun Street, Haidian District, 100081 Beijing, People's Republic of China
Full list of author information is available at the end of the article

Liu *et al. EURASIP Journal on Advances in Signal Processing* (2016) 2016:133

Page 2 of 12

resolvable sources was limited by the number of consecutive integral lags in the co-array. In this article, as an extension, the fractional difference co-array (FrDCA) perspective is proposed by introducing two fractional factors, which can generate either fractional difference sensor position or conventional integral difference ones. Such an extension would bring some advantages for the wideband signal DOA estimation: the sub-bands with different center frequencies would be converted into a set of signal received from the fractional virtual sensors. Then, one could choose any element positions of interest to perform DOA estimation. As a result, the degree of freedom and the maximum number of resolvable sources are increased.

The article is organized as follows. In Section 2, the FrDCA model is proposed. Section 3 provides the wideband DOA estimation models by using FrDCA. Numerical simulation results are provided in Section 4. Then, Section 5 concludes this paper. Notations: we use lower-case bold characters to denote vectors (e.g. $\mathbf{a}$), upper-case bold characters for matrices (e.g. $\mathbf{A}$), and upper-case outline letters for set (e.g. $\mathbb{A}$). For a matrix $\mathbf{A}$, the symbols $\mathbf{A}^*, \mathbf{A}^T$, and $\mathbf{A}^H$ denote the complex conjugation, transpose, and conjugate transpose respectively. $diag\{\mathbf{A}\}$ denotes a column vector consisting of the main diagonal elements of matrix $\mathbf{A}$. $diag\{\mathbf{a}\}$ denotes a diagonal matrix that uses the elements of vector $\mathbf{a}$ as its diagonal elements. $vec\{\mathbf{A}\}$ denotes vectorization operator.

The symbol $\odot$ and $\otimes$ denote the Khatri-Rao product and Kronecker product, respectively. $|\mathbb{A}|$ denotes the cardinality of set $\mathbb{A}$, which is a measure of the number of elements of the set $\mathbb{A}$.

2 Fractional difference co-array

2.1 Array signal model

Consider a NLA with M sensors at locations $\mathbb{L} = \{l_1, l_2, \ldots, l_M\}$ in units of half a minimal wavelength (denoted as d_0). Assume that D far-field sources s_k impinge to the array from directions $\theta_k, k = 1, 2, \cdots, D$. Choosing an assumed sensor located at the origin of coordinates as the reference, the received data of the pth sensor can be expressed as:

$$x_p(t) = \sum_{k=1}^{D} s_k \left(t - l_p \Delta_k \right) + n_p(t) \tag{1}$$

where $\Delta_k = d_0 \sin(\theta_k)/c$, $n_p(t)$ is the uncorrelated additive Gaussian white noise of the pth sensor.

Based on array output model (1), assume that one can obtain an $M \times M$ generalized SOS matrix $\mathbf{G}_{XX}$, which can be a covariance matrix (CM) or some time-frequency SOS matrices, such as cyclic correlation matrix (CCM) [21], in different cases.

$$\mathbf{G}_{XX} = \mathbf{A}_{\mathbb{L}}(\mu_1 f, \theta) \mathbf{\Lambda} \mathbf{A}_{\mathbb{L}}^H(\mu_2 f, \theta) + \mathbf{W} \tag{2}$$

where μ_1 and μ_2 are two fractional factors; $\mathbf{W}$ is the total effect of noise, interfere and cross terms;

and $\mathbf{A}_{\mathbb{L}}(f, \theta)$ denotes the array manifold, which depends upon three parameters: the array formulation $\mathbb{L}$, the center frequency f, and the impinging DOAs θ:[1]

$$\mathbf{A}_{\mathbb{L}}(f, \theta) = \left[\mathbf{a}_{\mathbb{L}}(f, \theta_1), \mathbf{a}_{\mathbb{L}}(f, \theta_2), \cdots, \mathbf{a}_{\mathbb{L}}(f, \theta_D) \right]$$
$$\mathbf{a}_{\mathbb{L}}(f, \theta_k) = \left[\mathbf{a}_{l_1}(f, \theta_k), \cdots, \mathbf{a}_{l_M}(f, \theta_k) \right]^T \tag{3}$$
$$\mathbf{a}_{l_p}(f, \theta_k) = e^{j2\pi f l_p \Delta_k}$$

where $\mathbf{a}_{\mathbb{L}}(f, \theta_k)$ denotes the steering vector of array $\mathbb{L}$ corresponding to the direction of θ_k. Here, it should be noted that $\mathbf{\Lambda}$ is a $D \times D$ diagonal matrix. The motivation behind this diagonal form will be soon made clearly.

Then, we would introduce a basic property of vectorization operation that will be useful in the sequel. For a diagonal matrix $\mathbf{B}$,

$$vec\{\mathbf{ABC}\} = \left(\mathbf{C}^T \otimes \mathbf{A}\right) vec\{\mathbf{B}\}$$
$$= \left(\mathbf{C}^T \odot \mathbf{A}\right) diag\{\mathbf{B}\} \tag{4}$$

One can refer to Theorem 2 of [22] for detailed proof. Based on (4), $\mathbf{G}_{xx}$ can be vectorized into (5):

$$\mathbf{y} = vec\{\mathbf{G}_{XX}\}$$
$$= \left(\mathbf{A}_{\mathbb{L}}^*(\mu_1 f, \theta) \odot \mathbf{A}_{\mathbb{L}}(\mu_2 f, \theta)\right) diag\{\mathbf{\Lambda}\} + vec\{\mathbf{W}\} \tag{5}$$
$$= \hat{\mathbf{A}}(f, \theta)\mathbf{p} + \mathbf{w}$$

where $\mathbf{p} = diag\{\mathbf{\Lambda}\}$, $\mathbf{w} = vec\{\mathbf{W}\}$, and $\hat{\mathbf{A}}(f, \theta) = \left(\mathbf{A}_{\mathbb{L}}^*(\mu_2 f, \theta) \odot \mathbf{A}_{\mathbb{L}}(\mu_1 f, \theta)\right)$. We will further analyze the term $\hat{\mathbf{A}}(f, \theta)$ by choosing two elements (e.g. pth, qth):

$$\mathbf{a}_{l_p}(\mu_1 f, \theta_k)\mathbf{a}_{l_q}^*(\mu_2 f, \theta_k) = e^{j2\pi \mu_1 f l_p \Delta_k} e^{-j2\pi \mu_2 f l_q \Delta_k}$$
$$= e^{j2\pi f(\mu_1 l_p - \mu_2 l_q)\Delta_k} \tag{6}$$
$$= \mathbf{a}_{c_{p,q}}(f, \theta)$$

where $c_{p,q} = \mu_1 l_p - \mu_2 l_q$. Let us form all the elements into a matrix form as (7):

$$\mathbf{A}_{\mathbb{L}}^*(\mu_2 f, \theta) \odot \mathbf{A}_{\mathbb{L}}(\mu_1 f, \theta) = \mathbf{A}_{\mu_2 \mathbb{L}}^*(f, \theta) \odot \mathbf{A}_{\mu_1 \mathbb{L}}(f, \theta)$$
$$\Rightarrow \mathbf{A}_{\mu_1 \mathbb{L} - \mu_2 \mathbb{L}}(f, \theta) \tag{7}$$

One can get the following two conclusions from Eqs. (5)~(7).

Firstly, for an array/co-array signal model, a scaled change in the center frequency can be equivalent to a same scaled change in the element positions. This concept is the basic transformation strategy to perform DOA estimation of wideband signal in Section 3.2.

Secondly, the left items of (7) can be viewed as an augmented manifold of a virtual array with sensors located at $\mathbb{D}, \mathbb{D} = \mu_1 \mathbb{L} - \mu_2 \mathbb{L}$. Compared to $\hat{\mathbf{A}}(f, \theta)$, $\mathbf{A}_{\mu_1 \mathbb{L} - \mu_2 \mathbb{L}}(f, \theta)$ only includes all the distinct rows of $\hat{\mathbf{A}}(f, \theta)$; therefore, one can obtain $\mathbf{A}_{\mu_1 \mathbb{L} - \mu_2 \mathbb{L}}(f, \theta) = \hat{\mathbf{S}}\hat{\mathbf{A}}(f, \theta)$, where $\hat{\mathbf{S}}$ is a $|\mathbb{D}| \times |\mathbb{L}|^2$ dimensional selection matrix.

Liu *et al. EURASIP Journal on Advances in Signal Processing* (2016) 2016:133

Page 3 of 12

2.2 Fractional difference co-array perspective

According to the above data model, we then propose the perspective and definition of FrDCA.

Definition 1 *[Fractional difference co-array]: Let us consider an array consisting of M sensors at positions* $\mathbb{A}$, $\mathbb{A} = \{a_1, a_2, ..., a_N\}$, *and then, for two given fractional factors* μ_1 *and* μ_2, *the fractional difference co-array is defined as the array consisting of a set of sensors at positions* $\mathbb{D}(\mu_1, \mu_2)$:

$$
\begin{aligned}
\mathbb{D}(\mu_1, \mu_2) &\triangleq \mu_1 \mathbb{A} - \mu_2 \mathbb{A} \\
&\triangleq \{c_{i,j} = \mu_1 a_i - \mu_2 a_j, \forall 1 \leq i, j \leq M\}
\end{aligned} \tag{8}
$$

For any two physical sensors at locations $\{a_i, a_j\}$, Fig. 1 shows three kinds of co-arrays. Obviously, for any two physical sensors, their DCA and SCA are uniquely defined, while the FrDCA is dependent on μ_1 and μ_2. As we know, any two numbers μ_1 and μ_2 can be expressed as $\mu_1 = \alpha + \beta$ and $\mu_2 = \alpha - \beta$. Therefore, three situations are analyzed and compared according to different α and β:

1. $\alpha \neq 0, \beta \neq 0$. For any pair-wise element positions, $c_{i,j}$ and $c_{j,i}$, one can obtain:

$$
\begin{aligned}
c_{i,j} &= \beta(a_i + a_j) + \alpha(a_i - a_j) \\
c_{j,i} &= \beta(a_i + a_j) - \alpha(a_i - a_j)
\end{aligned} \tag{9}
$$

   Equation (9) indicates that $c_{i,j}$ and $c_{j,i}$ are symmetrical with respect to the $\beta(a_i + a_j)$-dot. Since the $(a_i + a_j)$ for different index i, j is varied, the FrDCA geometry is asymmetrical in this case.

2. $\alpha \neq 0, \beta = 0$; The pair-wise element positions can be expressed as $c_{i,j} = \alpha(a_i - a_j) = -c_{j,i}$, which indicates that the FrDCA geometry is symmetrical with respect to the fixed zero-dot. Furthermore, if $\alpha = 1$, then $c_{i,j} = (a_i - a_j) = -c_{j,i}$. The FrDCA becomes a conventional DCA proposed in [10]. For a given α, the corresponding FrDCA is a α-scaled conventional DCA, $\mathbb{D}(\alpha, \alpha) = \alpha \mathbb{D}(1, 1)$. Combing with (7), given a
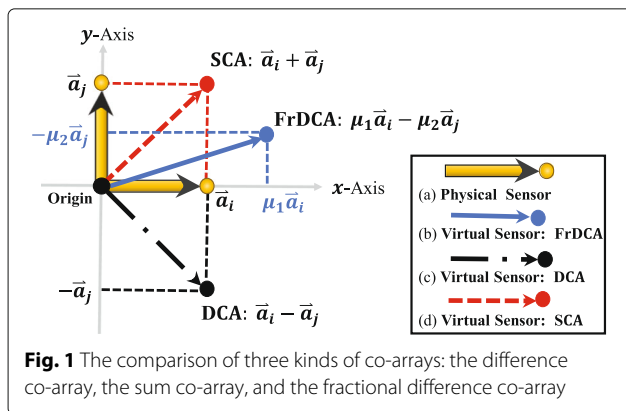
reference frequency f and an operation frequency f_k, then one can obtain a α-scaled FrDCA $\mathbb{D}(\alpha_k, \alpha_k)$, where $\alpha_k = f_k/f$. As a result, any desired virtual sensor position can be generated by choosing an appropriate operation frequency f_k. In a sense, such FrDCA generated by multi-frequencies operation has been utilized in [16, 17] to fill the missing co-array elements, thereby enabling the co-prime array to effectively utilize all of the offered DOFs.

3. $\beta \neq 0, \alpha = 0$; The pair-wise element positions can be expressed as $c_{i,j} = \beta(a_i + a_j) = c_{j,i}$, which indicates that the redundancy of any virtual sensor position is no less than two. Furthermore, if $\beta = 1$, then $c_{i,j} = (a_i + a_j) = c_{j,i}$. The FrDCA becomes a SCA. For a given β, it is easy to find that the corresponding FrDCA is a β-scaled SCA, $\mathbb{D}(\beta, -\beta) = \beta \mathbb{D}(1, -1)$.

3 DOA estimation by using FrDCA

3.1 Review of narrowband signal based DCA model

The conventional DCA perspective was proposed in [10]. Assume that the impinging source in (1) can be view as a narrowband uncorrelated model; hence, the array output can be expressed as

$$
\mathbf{X}(t) = \mathbf{A}_{\mathbb{L}}(f, \theta)\mathbf{s}(t) + \mathbf{n}(t) \tag{10}
$$

where f denotes the center frequency and $\mathbf{s}(t)$ and $\mathbf{n}(t)$ are the source vector and noise vector, respectively. By collecting N snapshots, the covariance matrix can be estimated by (11)

$$
\begin{aligned}
\mathbf{R}_{xx} &\triangleq E\{\mathbf{X}\mathbf{X}^H\} \approx \frac{1}{N} \sum_{t=1}^{N} \mathbf{X}(t)\mathbf{X}(t)^H \\
&= \mathbf{A}_{\mathbb{L}}(f, \theta)\mathbf{R}_{ss}\mathbf{A}_{\mathbb{L}}^H(f, \theta) + \sigma^2 \mathbf{I_M}
\end{aligned} \tag{11}
$$

where $\mathbf{I_M}$ denotes an $M \times M$ identity matrix, $\mathbf{R}_{ss}$ the estimated covariance matrix of source signal, which is a diagonal matrix. It is entirely suited to the model in (2) with $\mu_1 = \mu_2 = 1$.

$$
\begin{aligned}
\mathbf{y} &= vec\{\mathbf{R}_{xx}\} \\
&= \left(\mathbf{A}_{\mathbb{L}}^*(f, \theta) \odot \mathbf{A}_{\mathbb{L}}(f, \theta)\right)\mathbf{p} + \sigma^2 vec\{\mathbf{I_M}\} \\
&= \mathbf{A}_{\text{DCA}}(f, \theta)\mathbf{p} + \sigma^2 \mathbf{1_M}
\end{aligned} \tag{12}
$$

where $\mathbf{1_M} = vec\{\mathbf{I_M}\}$, $\mathbf{p} = diag\{\mathbf{R}_{ss}\}$ and the corresponding DCA can be expressed as $\mathbb{D}(1, 1) = \{l_i - l_j, 1 \leq i, j \leq M\}$.

After obtaining the virtual array signal model in (12), all the impinging DOAs can be estimated by using the spatial smoothing MUSIC algorithm or the compressive sensing (CS) algorithm, which have been discussed in [10–14].

Fig. 1 The comparison of three kinds of co-arrays: the difference co-array, the sum co-array, and the fractional difference co-array

Liu *et al. EURASIP Journal on Advances in Signal Processing* (2016) 2016:133

Page 4 of 12

3.2 Wideband signal-based FrDCA model

In practice, some wideband signal applications, such as the spread spectrum communication and ultrawideband radar system, have been increasing recently. DOA estimation for such a wideband signal is also required. For a wideband signal, the envelope is distinct at different sensors; therefore, the array outputs cannot be simply formed into a matrix form as (10). The received signal from each sensor can be divided into m independent sub-bands with different center frequencies by performing discrete Fourier transform (DFT). Assume that their center frequencies are denoted as $\{f_1, f_2, ...f_m\}$. Then, by choosing a center frequency f_c as a reference, the ith frequency can be normalized as $f_i = \alpha_i f_c$, where α_i is a fractional ratio. For a given array structure $\mathbb{L}$, the ith sub-band signal can be denoted as

$$\mathbf{X}_i = \mathbf{A}_{\mathbb{L}}(f_i, \theta)\mathbf{S}_i + \mathbf{W}_i \tag{13}$$

where $i = 1, 2, \cdots, m$; $f_i, \mathbf{S}_i$, and $\mathbf{W}_i$ denote the center frequency, source vector, and noise vector of the ith sub-band signal, respectively. Then, the covariance matrix can be formed by (14)

$$\begin{aligned}\mathbf{R}_{xx}(f_i) &= \mathbf{A}_{\mathbb{L}}(f_i, \theta)\mathbf{R}_{ss}(f_i)\mathbf{A}_{\mathbb{L}}^H(f_i, \theta) + \sigma_{n_i}^2 \mathbf{I_M} \\ &= \mathbf{A}_{\mathbb{L}}(\alpha_i f_c, \theta)\mathbf{R}_{ss}(f_i)\mathbf{A}_{\mathbb{L}}^H(\alpha_i f_c, \theta) + \sigma_{n_i}^2 \mathbf{I_M}\end{aligned} \tag{14}$$

where $\mathbf{R}_{ss}(f_i)$ is a diagonal matrix under the assumption of uncorrelated sources for each frequency f_i, $\mathbf{R}_{ss}(f_i) = diag\left\{\left[\begin{array}{cccc}\delta_{s_i,1}^2 & \delta_{s_i,1}^2 & \cdots & \delta_{s_i,D}^2\end{array}\right]\right\}$, $\delta_{s_i,k}^2$ is the power of kth source at ith sub-band. All the signal power can be estimated by averaging the diagonal elements of $\mathbf{R}_{ss}(f_i)$:

$$\bar{\delta}^2(f_i) = \frac{1}{M}\sum_{i=1}^{M}[\mathbf{R}_{ss}(f_i)]_{i,i} \tag{15}$$

Unlike the case of narrowband single frequency, Eq. (14) would be vectorized into (16) combing with an operation of signal power adjustment:

$$\begin{aligned}\mathbf{y}(f_i) &= vec\{\mathbf{R}_{xx}(f_i)/\bar{\delta}^2(f_i)\} \\ &= (\mathbf{A}_{\mathbb{L}}^*(\alpha_i f_c, \theta) \odot \mathbf{A}_{\mathbb{L}}(\alpha_i f_c, \theta))\mathbf{p}_i + \gamma_{n_i} vec\{\mathbf{I_M}\} \\ &= \hat{\mathbf{A}}_i(f_c, \theta)\mathbf{p}_i + \gamma_{n_i}\mathbf{1_M} \in \mathbb{C}^{M^2 \times 1}\end{aligned} \tag{16}$$

where $\mathbf{p}_i = diag\{\mathbf{R}_{ss}(f_i)/\bar{\delta}^2(f_i)\} = \left[\begin{array}{ccc}\gamma_{s_i,1} & \cdots & \gamma_{s_i,D}\end{array}\right]^T$, $\gamma_{s_i,k} = \delta_{s_i,k}^2/\bar{\delta}^2(f_i)$. Compared to the signal power $\delta_{s_i,k}^2$, $\gamma_{s_i,k}$ is a ratio, which indicates the level of the kth signal power to the level of total received signal power (including noise power) in the ith sub-band.

Based on the model in (16), the corresponding FrDCA can be $\mathbb{D}_i(\alpha_i, \alpha_i)$. Due to the redundancy of the co-array, $|\mathbb{D}_i(\alpha_i, \alpha_i)| \leq M(M-1)$, one can average the repeated rows and reduce the M^2 dimensional model in (16) into a $|\mathbb{D}_i|$ dimensional model in (17):

$$\begin{aligned}\mathbf{y}_{\mathbb{D}_i}(f_i) &= \mathbf{A}_{\mathbb{D}_i}(f_c, \theta)\mathbf{p}_i + \gamma_{n_i}\mathbf{e}_{\mathbb{D}_i} \\ &= \left[\mathbf{A}_{\mathbb{D}_i}(f_c, \theta)\ \mathbf{e}_{\mathbb{D}_i}\right]\left[\begin{array}{c}\mathbf{p}_i \\ \gamma_{n_i}\end{array}\right] \in \mathbb{C}^{|\mathbb{D}_i| \times 1} \\ &= \hat{\mathbf{A}}_{\mathbb{D}_i}(f_c, \theta)\hat{\mathbf{p}}_i\end{aligned} \tag{17}$$

where $\mathbf{e}_{\mathbb{D}_i} = \left[\begin{array}{ccc}\mathbf{0}_{1 \times \frac{|\mathbb{D}_i|-1}{2}} & 1 & \mathbf{0}_{1 \times \frac{|\mathbb{D}_i|-1}{2}}\end{array}\right]^T$; $\hat{\mathbf{A}}_{\mathbb{D}_i}(f_c, \theta) = \left[\mathbf{A}_{\mathbb{D}_i}(f_c, \theta)\ \mathbf{e}_{\mathbb{D}_i}\right]$ behaves like an augmented array manifold containing a virtual array manifold matrix $\hat{\mathbf{A}}_{\mathbb{D}_i}(f_c, \theta)$; and a noise-related vector $\mathbf{e}_{\mathbb{D}_i}$; $\hat{\mathbf{p}}_i = \left[\begin{array}{cc}\mathbf{p}_i^T & \gamma_{n_i}\end{array}\right]^T$ behaves like an equivalent input signal, which is only dependent on the proportion of each signal power.

The reduced model in (17) is a complex valued signal model generated by averaging the element of covariance matrix. As we know, for the covariance matrix, $\mathbf{R}_{xx}(i,j) = \mathbf{R}_{xx}(j,i)^*$. Therefore, if we let the elements of set $\mathbb{D}_i$ to be listed in an ascending order, one can separate the real and imaginary parts of $\mathbf{y}_{\mathbb{D}_i}(f_i)$ by making use of the conjugate symmetry of covariance matrix :

$$\begin{aligned}\Re(\mathbf{y}_{\mathbb{D}_i}) &= \frac{\mathbf{y}_{\mathbb{D}_i} + \mathbf{J}_{|\mathbb{D}_i|}\mathbf{y}_{\mathbb{D}_i}}{2} = \frac{\mathbf{I}_{|\mathbb{D}_i|} + \mathbf{J}_{|\mathbb{D}_i|}}{2}\hat{\mathbf{A}}_{\mathbb{D}_i}(f_c, \theta)\hat{\mathbf{p}}_i \\ \Im(\mathbf{y}_{\mathbb{D}_i}) &= \frac{\mathbf{y}_{\mathbb{D}_i} - \mathbf{J}_{|\mathbb{D}_i|}\mathbf{y}_{\mathbb{D}_i}}{2j} = \frac{\mathbf{I}_{|\mathbb{D}_i|} - \mathbf{J}_{|\mathbb{D}_i|}}{2j}\hat{\mathbf{A}}_{\mathbb{D}_i}(f_c, \theta)\hat{\mathbf{p}}_i\end{aligned} \tag{18}$$

where $\mathbf{J}_{|\mathbb{D}_i|}$ denotes a $|\mathbb{D}_i| \times |\mathbb{D}_i|$ dimensional exchange matrix. For the model (18), there are two important remarks.

Firstly, we focus on $\hat{\mathbf{A}}_{\mathbb{D}_i}$. Based on the definition of $\mathbb{D}_i(\alpha_i, \alpha_i)$ in (8), one can obtain that the elements in $\mathbb{D}_i(\alpha_i, \alpha_i)$ are pair-wise, $c_{i,j} = -c_{j,i}$, which leads that the corresponding steering vectors are conjugate, $\mathbf{a}_{c_{i,j}} = \mathbf{a}_{c_{j,i}}^*$. Therefore, $\hat{\mathbf{A}}_{\mathbb{D}_i} + \mathbf{J}_{|\mathbb{D}_i|}\hat{\mathbf{A}}_{\mathbb{D}_i}$ is the real-valued matrix, while $\hat{\mathbf{A}}_{\mathbb{D}_i} - \mathbf{J}_{|\mathbb{D}_i|}\hat{\mathbf{A}}_{\mathbb{D}_i}$ is the imaginary valued matrix.

Secondly, we focus on $\Re(\mathbf{y}_{\mathbb{D}_i})$ and $\Im(\mathbf{y}_{\mathbb{D}_i})$. The elements of these two real-valued vectors are symmetric character sequences, respectively. Therefore, one can construct a real-valued signal model as (19) by selecting the first $\frac{|\mathbb{D}_i|+1}{2}$ rows of $\Re(\mathbf{y}_{\mathbb{D}_i})$ and the first $\frac{|\mathbb{D}_i|-1}{2}$ rows of $\Im(\mathbf{y}_{\mathbb{D}_i})$

$$\begin{aligned}\mathbf{z}(f_i) &= \left[\begin{array}{c}\mathbf{S}_R\Re(\mathbf{y}_{\mathbb{D}_i}) \\ \mathbf{S}_I\Im(\mathbf{y}_{\mathbb{D}_i})\end{array}\right] = \underbrace{\left[\begin{array}{c}\frac{\mathbf{S}_R + \mathbf{S}_R\mathbf{J}_{|\mathbb{D}_i|}}{2} \\ \frac{\mathbf{S}_I - \mathbf{S}_I\mathbf{J}_{|\mathbb{D}_i|}}{2j}\end{array}\right]\hat{\mathbf{A}}_{\mathbb{D}_i}(f_c, \theta)}_{\mathbf{B}_{\mathbb{D}_i}(f_c, \theta)}\hat{\mathbf{p}}_i \\ &= \mathbf{B}_{\mathbb{D}_i}(f_c, \theta)\hat{\mathbf{p}}_i \in \mathbb{R}^{|\mathbb{D}_i| \times 1}\end{aligned} \tag{19}$$

where $\mathbf{S}_R$ and $\mathbf{S}_I$ are selection matrices for the real and imaginary parts, respectively:

$$\begin{aligned}\mathbf{S}_R &= [\ \mathbf{I}_{\frac{|\mathbb{D}_i|+1}{2}}\ \mathbf{0}_{\frac{|\mathbb{D}_i|+1}{2} \times \frac{|\mathbb{D}_i|-1}{2}}\ ] \in \mathbb{R}^{\frac{|\mathbb{D}_i|+1}{2} \times |\mathbb{D}_i|} \\ \mathbf{S}_I &= [\ \mathbf{I}_{\frac{|\mathbb{D}_i|-1}{2}}\ \mathbf{0}_{\frac{|\mathbb{D}_i|-1}{2} \times \frac{|\mathbb{D}_i|+1}{2}}\ ] \in \mathbb{R}^{\frac{|\mathbb{D}_i|-1}{2} \times |\mathbb{D}_i|}\end{aligned} \tag{20}$$

Liu *et al. EURASIP Journal on Advances in Signal Processing* (2016) 2016:133

Page 5 of 12

Based on this real-valued signal model in (20), the output signals $\mathbf{z}(f_i)$ corresponding to different frequencies share the same spatial support. Therefore, without loss of generality, joint sparse recovery (joint CS) techniques can be applied for DOA estimation:

$$
\begin{aligned}
\mathbf{Z}_1 &= \left| \; \mathbf{z}(f_1)^T \; \mathbf{z}(f_2)^T \; \cdots \; \mathbf{z}(f_m)^T \; \right|^T \\
&= \underbrace{\left| \begin{matrix} \mathbf{B}_{\mathbb{D}_1}(f_c, \theta) & \cdots & \mathbf{0} \\ \vdots & \ddots & \vdots \\ \mathbf{0} & \cdots & \mathbf{B}_{\mathbb{D}_m}(f_c, \theta) \end{matrix} \right|}_{\boldsymbol{\Phi}_1(f_c, \theta)} \left| \begin{matrix} \hat{\mathbf{p}}_1 \\ \vdots \\ \hat{\mathbf{p}}_m \end{matrix} \right| \\
&= \boldsymbol{\Phi}_1(f_c, \theta) \tilde{\mathbf{p}}_1 \in \mathbb{R}^{L_1 \times 1}
\end{aligned}
\tag{21}
$$

where $L_1 = m|\mathbb{D}_1|$, $\tilde{\mathbf{p}}_1 = [\hat{\mathbf{p}}_1^T \; \hat{\mathbf{p}}_2^T \; \cdots \; \hat{\mathbf{p}}_m^T]^T$, $\boldsymbol{\Phi}_1(f_c, \theta)$ is a block diagonal matrix. (21) is a joint sparse DOA reconstruction model without considering signal properties.

If the ratio of each signal power can be independent of frequency f_i, $\hat{\mathbf{p}}_i = \bar{\mathbf{p}}_1$, $i = 1, 2, ..., m$, all the vectorized signals in (16) can be directly stacked into a longer virtual signal in (22) and an augmented FrDCA in (23):

$$
\begin{aligned}
\mathbf{Z}_1 &= \left| \; \mathbf{z}(f_1)^T \; \mathbf{z}(f_2)^T \; \cdots \; \mathbf{z}(f_m)^T \; \right|^T \\
&= \left| \; \mathbf{B}_{\mathbb{D}_1}(f_c, \theta)^T \; \cdots \; \mathbf{B}_{\mathbb{D}_m}(f_c, \theta)^T \; \right|^T \bar{\mathbf{p}}_1 \\
&= \boldsymbol{\Psi}_1(f_c, \theta) \bar{\mathbf{p}}_1 \in \mathbb{R}^{L_1 \times 1}
\end{aligned}
\tag{22}
$$

where $\boldsymbol{\Psi}_1(f_c, \theta)$ behaves like a $L_1 \times D$ dimensional sampling matrix and $\mathbf{Z}_1$ and $\bar{\mathbf{p}}_1$ denotes input signal and output signal, respectively.

$$
\overline{\mathbb{D}}_1 = \bigcup_{i=1}^{m} \{ \mathbb{D}_i(\alpha_i, \alpha_i) \} = \bigcup_{i=1}^{m} \{ \alpha_i \mathbb{L} - \alpha_i \mathbb{L} \}
\tag{23}
$$

3.3 Sparse DOA recovery algorithm
After obtaining the array model in (21) and (22), DOA estimation can be performed mainly based on two methodologies: compressive sensing (CS) and subspace fitting (SSF).

Choosing the CS methodology, by dividing the region of interest into a finite grid $\hat{\theta}$, where $\hat{\theta} = \{\hat{\theta}_1, \hat{\theta}_2, \cdots, \hat{\theta}_Q\}$, one could establish an augmented array manifold $\mathbf{A}_{\mathbb{D}_i}(f_c, \hat{\theta})$ and further build the corresponding over-complete dictionaries $\boldsymbol{\Phi}_i(f_c, \hat{\theta})$ and $\boldsymbol{\Psi}_i(f_c, \hat{\theta})$. Equation (21) can be rewritten as (24)

$$
\mathbf{Z}_1 = \boldsymbol{\Phi}_1(f_c, \hat{\theta}) \tilde{\mathbf{p}}_1(\hat{\theta}) \in \mathbb{R}^{L_1 \times 1}
\tag{24}
$$

where $\boldsymbol{\Phi}_1(f_c, \hat{\theta}) \in \mathbb{R}^{L_1 \times m(Q+1)}$ and $\tilde{\mathbf{p}}_1(\hat{\theta}) \in \mathbb{R}^{m(Q+1) \times 1}$. Since $Q \gg D$, the signal $\hat{\mathbf{p}}_i$ is a D sparse vector in this setting. Then, the general objective function for this problem is (25)

$$
\begin{aligned}
& \min \left\| \tilde{\mathbf{p}}_1^\circ(\hat{\theta}) \right\|_1 \\
& \text{subject to } \left\| \mathbf{Z}_1 - \boldsymbol{\Phi}_1(f_c, \hat{\theta}) \tilde{\mathbf{p}}_1(\hat{\theta}) \right\|_2 \leq \epsilon
\end{aligned}
\tag{25}
$$

where $\tilde{\mathbf{p}}_1^\circ(\hat{\theta}) = \sum_{\ell=0}^{m-1} \| \tilde{\mathbf{p}}_1((Q+1)\ell+1 \; : \; (Q+1)\ell+Q) \|_1$ and ϵ denotes the error tolerance of noise dependence. Similarly, (22) also can be rewritten as (26)

$$
\mathbf{Z}_1 = \boldsymbol{\Psi}_1(f_c, \hat{\theta}) \bar{\mathbf{p}}_1(\hat{\theta}) \in \mathbb{R}^{L_1 \times 1}
\tag{26}
$$

where $\boldsymbol{\Psi}_1(f_c, \hat{\theta}) \in \mathbb{R}^{L_1 \times (Q+1)}$ and $\bar{\mathbf{p}}_1(\hat{\theta}) \in \mathbb{R}^{(Q+1) \times 1}$. The general objective function for this problem is (27)

$$
\begin{aligned}
& \min \left\| \bar{\mathbf{p}}_1(\hat{\theta}) \right\|_1 \\
& \text{subject to } \left\| \mathbf{Z}_1 - \boldsymbol{\Psi}_1(f_c, \hat{\theta}) \bar{\mathbf{p}}_1(\hat{\theta}) \right\|_2 \leq \epsilon
\end{aligned}
\tag{27}
$$

To solve this problem, LASSO [23] is an effective algorithm. The objective function can be expressed as

$$
\bar{\mathbf{p}}_1 = \min_{\bar{\mathbf{p}}_1} \frac{1}{2} \| \mathbf{Z}_1 - \boldsymbol{\Psi}_1(f_c, \hat{\theta}) \bar{\mathbf{p}}_1(\hat{\theta}) \|_2 + \eta \| \bar{\mathbf{p}}_1(\hat{\theta}) \|_1
\tag{28}
$$

where η is the penalty parameter of data dependence.

In the model (24) and (26), $\mathbf{Z}_1$ is influenced by noise power $\gamma_{n,i}$. In order to avoid estimating noise power, one can remove all the zero-lag entities. As a result, the noise vector $\mathbf{e}_{\mathbb{D}_i}$ in (17) can be removed accordingly. This operation would reduce one dimension of the over-complete dictionaries and slightly decrease the computation complexity.

If choosing the SSF methodology, which requires a set of uniformly distributed sensors, one could select and construct a virtual ULA $\overline{\mathbb{U}}$,

$$
\overline{\mathbb{U}} = \{ -L_u, \; -L_u+1, \; \cdots, \; L_u-1, \; L_u \}
\tag{29}
$$

Strictly speaking[2], $\overline{\mathbb{U}}$ should be a subset of $\overline{\mathbb{D}}_1$ so that the corresponding virtual signal $\mathbf{Y}_u$ received by the ULA $\overline{\mathbb{U}}$ can be exactly selected from $\mathbf{Y}_1$,

$$
\mathbf{Y}_u = \mathbf{S}_u \mathbf{Y}_1 = \mathbf{A}_{\overline{\mathbb{U}}}(f, \theta) \bar{\mathbf{p}}_1 \in \mathbb{C}^{(2L_u+1) \times 1}
\tag{30}
$$

where $\mathbf{Y}_1 = \left[\mathbf{y}_{\mathbb{D}_1}^T, \cdots, \mathbf{y}_{\mathbb{D}_m}^T \right]^T$ and $\mathbf{S}_u$ is a $(2L_u + 1) \times L_1$ dimensional selection matrix. In this setting, (30) behaves like a fully coherent ULA signal model; therefore, MUSIC algorithm combined with a rank restoring method [24, 25] can be applied to obtain a spatial spectra $\mathbf{P}(\tilde{\theta})$,

$$
\mathbf{P}(\tilde{\theta}) = \frac{1}{||\mathbf{a}_{\overline{\mathbb{U}}}(\tilde{\theta}, f)^H \mathbf{U}_n||^2}
\tag{31}
$$

where $\mathbf{U}_n$ is the eigenvector of noise space, which can be estimated by performing eigenvalue decomposition of the rank restored covariance matrix.

3.4 Related remarks
In this paper, we start from providing a new FrDCA concept. Compared to the prior proposed DCA concept, the position of virtual sensor can be generated from not only the conventional consecutive integral co-sensors but also the fractional ones. Therefore, in a sense, it can be viewed

as an extended or generalized virtual co-array concept. This relationship is intuitively illustrated in Fig. 1. Then, by using FrDCA perspective, the virtual co-array can be extended into the wideband signal case. A wideband signal can be divided into several narrow sub-bands (with different center frequencies), which can be further transformed into a group of signals (with a fixed center frequency) received from a virtual array.

On the wideband co-array model: to solve the problem of wideband signal DOA estimation, generally, the signal would be divided into many sub-bands with different center frequencies. Therefore, how to combine such multi-frequency sub-bands is the central problem. The authors in [20] combined the signal subspaces at different frequencies into one joint subspace at the chosen frequency by introducing an auto-focusing matrix. Combing with the sparse array configuration, theoretically, more wideband sources than physical sensors can be resolved. However, the subspace information of many sub-bands was not been fully utilized due to the auto-focusing technique, which just cast all the subspaces into a joint one with a desired center frequency. By using the proposed FrDCA concept, all the sub-bands can be fully utilized to generate virtual sensors and to increase the DOF capacity. Therefore, the proposed algorithm can resolve more wideband sources than sensors (even than the DCA-based uniformly virtual co-sensors). These advantages would be validated in the following simulation section.

On the sparse recovery model: in this paper, by utilizing the conjugated-symmetrical property of the virtual signal model, we establish a real-valued sparse recovery model. Therefore, compared to the prior proposed complex valued sparse recovery model in [17, 18, 20, 26], the computation complexity is reduced.

The author in [16, 17] proposed a multi-frequency co-prime array concept. This technique requires to actively transmit/receive some narrowband signals with different frequencies in different time slots, so that the covariance matrices of the received signals can exactly fill the missed holes in the co-array, as a result, the DOF capacity of co-array can be enhanced accordingly. In this active-like scheme, the center frequencies and time slots must be pre-planed before transmitting the certain waveforms. The proposed algorithm just requires to receive a wideband signal, which behaves more like a passive scheme. As a result, no such pre-planed time slot is required and the center frequencies can be accordingly chosen/adjusted after receiving the wideband signal. In addition, the prior multi-frequency technique only make use of the position of integral virtual sensor. For the proposed technique, all the positions including fractional ones can be directly presented and utilized. One can select any sensors of interest by adjusting a particular center frequency.

Therefore, the FrDCA concept provide a more flexible strategy.

How to properly select the center frequency f_k? For a given physical array $\mathbb{L}$ and a wideband signal, whose frequency spectrum of interest can cover from $f_{\min}$ to $f_{\max}$, one can uniquely determine $\mathbb{D}(1,1) = \mathbb{L} - \mathbb{L}$. Then, if one requires a sensor located at c_k, all the potential factors α_k are given by $c_k \in \alpha_k \mathbb{D}(1,1), \alpha_k \in \frac{c_k}{\mathbb{D}(1,1)}$. Take the corresponding center frequency f_k and the bandwidth of sub-band ϖ_k into consideration, the constrain condition can be expressed as $f_{\min} \leq \alpha_k f_0 \pm 0.5\varpi_k \leq f_{\max}$. In practice, using the most adjacent sensor to fill this position is the best choice, which can result in the least frequency offset.

4 Numerical experiments

In this section, we conduct some numerical experiments by using MATLAB. To solve the (joint) CS problem, we use CVX toolbox, a package for specifying and solving convex programs [27, 28].

4.1 FrDCA-based MUSIC algorithm

In the first experiment, considering a NLA with sensors located at $\mathbb{L} = \{0, 1, 4, 10, 12, 17\}\frac{\lambda}{2}$ (where λ is the minimal wavelength of signal) and assuming that D Linear Frequency Modulated (LFM) sources with 10-MHz bandwidth and 20-MHz center frequency uniformly distributed in space from $-52°$ to $52°$, all the LFM sources have random initial phases and different initial frequencies in order to prevent coherence. Four thousand samples are collected at the sampling rate of 80 MHz for 50 μs. The SNR is 15 dB. The frequency spectrum of interest is from 15 to 25 MHz. Firstly, we focus on the conventional difference co-array $\mathbb{D}(1,1) = \mathbb{L} - \mathbb{L}$. The positions of the virtual sensors and the corresponding redundancy are illustrated in Fig. 2a. Obviously, its consecutive lags are from -13 to 13. There are holes at positions ± 14 and ± 15. The aforementioned analyses have pointed out that $\mathbb{D}(\alpha_k, \alpha_k)$ is the α_k-scaled $\mathbb{D}(1,1)$. Therefore, in order to fill the holes at positions ± 14, there are many potential choices for α_k, such as $\frac{14}{17}, \frac{14}{16}, \frac{14}{13}$, and so on. Combing all the holes into consideration, we divide the wideband signal into the following eight sub-bands with α_k being $\{\frac{14}{16}, \frac{15}{16}, \frac{16}{16}, \frac{18}{16}, \frac{19}{16}, \frac{20}{16}, \frac{22}{16}\}$. The corresponding center frequencies can be $\alpha_k f_0$, where f_0 is the reference center frequency. All the selected center frequencies should be within the frequency spectrum of interest, 15 MHz $\leq$ $\alpha_k f_0$ $\leq$ 25 MHz. Under this constraint, we can chose f_0 = 18 MHz. The corresponding center frequency f_k = $\{15.75, 16.875, 18.00, 20.25, 21.375, 22.50, 23.625, 24.75\}$ MHz. Figure 2b shows all the positions of the virtual sensors in eight kinds of FrDCAs. In addition, in order to make the sub-bands satisfy narrowband requirement, the
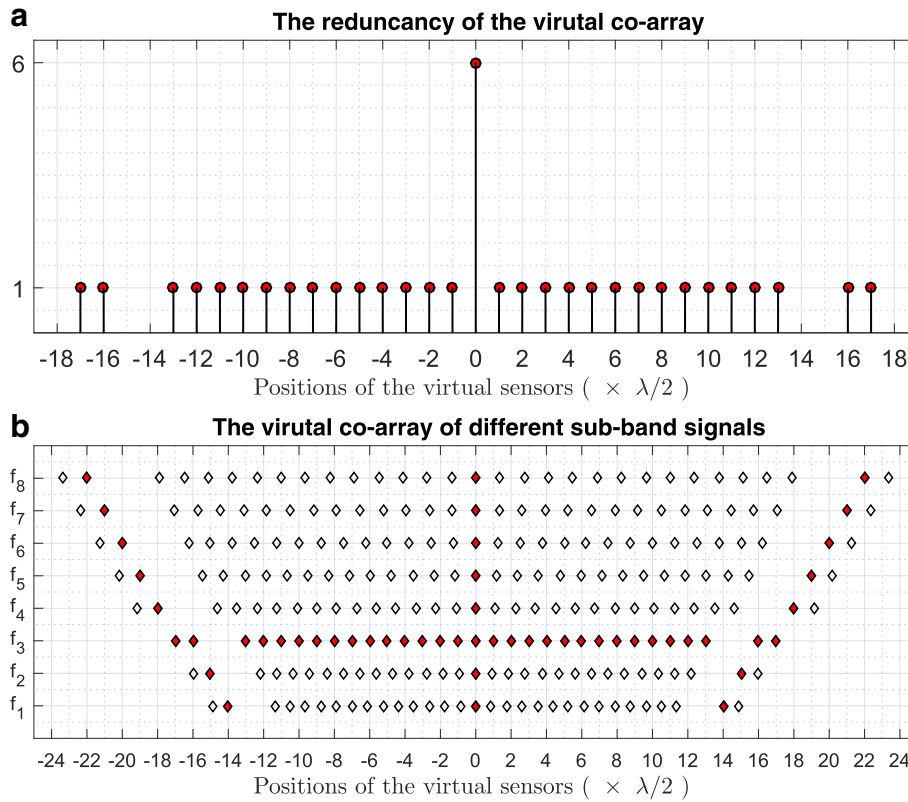
a The reducnancy of the virutal co-array

b The virutal co-array of different sub-band signals

Fig. 2 The positions of virtual sensors. **a** The conventional DCA $\mathbb{D}(1,1)$ and the corresponding redundancy and **b** FrDCA $\mathbb{D}(\alpha_k, \alpha_k)$ for different sub-band signals, where the selected uniformly distributed sensors $\overline{\mathbb{U}}$ are marked with red face color

bandwidth of each sub-band should be much less than the center frequency f_k. Therefore, we chose the bandwidth as 0.6 MHz.

For DOA estimation based on MUSIC algorithm, we can select a set of consecutive and uniformly distributed lags, as presented by the symbol $\diamond$ with red face color in Fig. 2b. The virtual ULA can be $\overline{\mathbb{U}} = \{-22, -21, \cdots, 21, 22\}$. Compared to the conventional DCA, the one-side aperture of virtual array is increased from 13 to 22. It validates that, by using the FrDCA concept, the wideband signal received from an array can be divided into a set of narrowband signal received from a larger aperture array with enhanced DOF capacity.

In the first experiment, consider nine uncorrelated LFM sources impinging to the array from the direction $\theta, \theta = \{-52°, -39°, \cdots, 39°, 52°\}$, and make a comparison with the auto-focusing based MUSIC algorithm in [20]. For auto-focusing-based MUSIC algorithm, in order to make fully use of all the virtual sensor, the correlation elements corresponding to the holes are assigned with zero. In this case, the virtual aperture can be increased to 17 other than 13. The MUSIC spectra of 30 independent trials for two kinds of algorithm are illustrated in Fig. 3. It shows that all the nine sources can be detected

by two algorithms. However, making a further comparison between the peaks of the spectra, the peaks on the FrDCA-based MUSIC spectra are much sharper, which means that the estimated results are more accurate and precise.

In the second experiment, increase the number of sources to 14, $\theta = \{-52°, -46°, \cdots, 46°, 52°\}$. The MUSIC spectra of 30 independent trials are illustrated in Fig. 4. It shows that the auto-focusing-based MUSIC algorithm cannot work in such a multi-source condition, while the FrDCA-based algorithm can clearly and correctly detect all the 14 sources.

4.2 FrDCA-based CS algorithm

In this section, we test the FrDCA-based CS algorithm. Compared to the MUSIC algorithm, it does not require the consecutive lags. Therefore, we chose α_k and f_0 as follows: $f_0 = 16$ MHz, $\alpha_k = \{\frac{15.3}{16}, \frac{16}{16}, \frac{18}{16}, \frac{19}{16}, \frac{20}{16}, \frac{21}{16}, \frac{22}{16}, \frac{23}{16}, \frac{24}{16}, \frac{24.7}{16}\}$. The other parameters are set as they are before. In this setting, a much larger virtual aperture is obtained.

In the third experiment, consider nine uncorrelated LFM sources and DOA estimation performed based on the two proposed sparse model in (25) and (28), where a
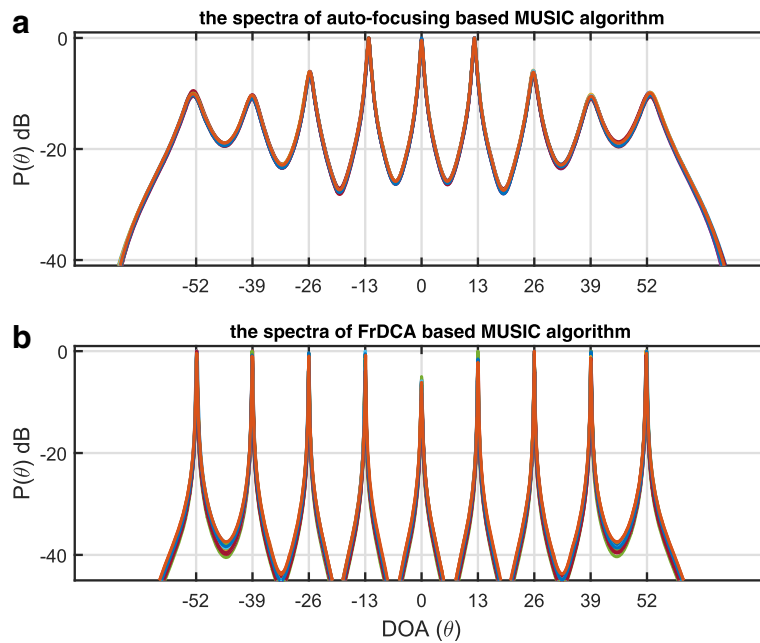
Liu *et al. EURASIP Journal on Advances in Signal Processing* (2016) 2016:133

Page 8 of 12

Fig. 3 The spectra of two algorithms: **a** the auto-focusing-based MUSIC and **b** the FrDCA-based MUSIC by using a six-element NLA from an environment containing nine wideband signals

grid interval of $\triangle\hat{\theta} = 0.25°$ and the penalty parameter of $\eta = 0.55$ are used. The normalized spectra of 30 independent trials for two kinds of CS algorithms are illustrated in Fig. 5. By using CVX toolbox to solve the two models at the same platform, based on the run-time information

of CVX, the total CPU time for CS model in (28) is 0.51 s, while 7.34 s for joint CS model in (25). Then, a further comparison on the spectra shows that, generally, the two algorithms can resolve all the sources clearly and correctly with some sharp peaks. Specifically, the joint CS algorithm
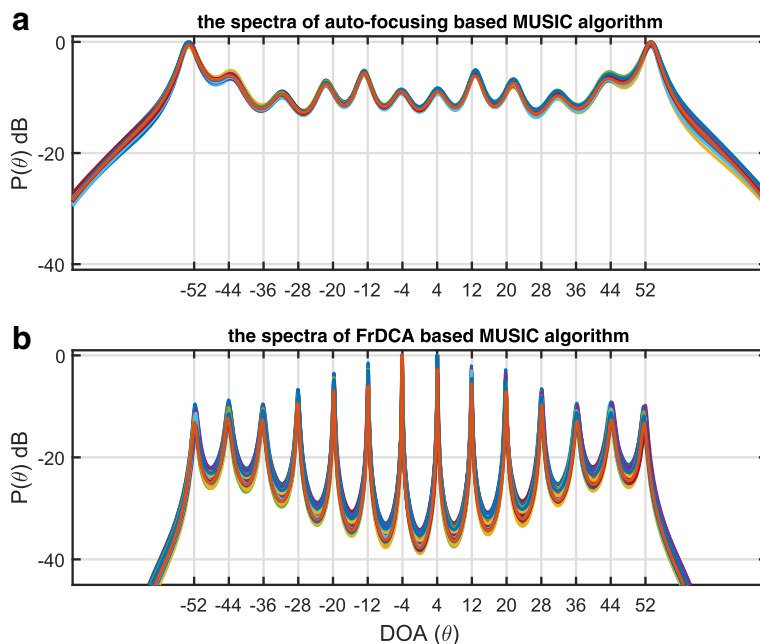
Fig. 4 The spectra of two algorithms: **a** the auto-focusing-based MUSIC **b** the FrDCA-based MUSIC algorithms by using a six-element NLA from an environment containing 14 wideband signals

Liu *et al. EURASIP Journal on Advances in Signal Processing* (2016) 2016:133
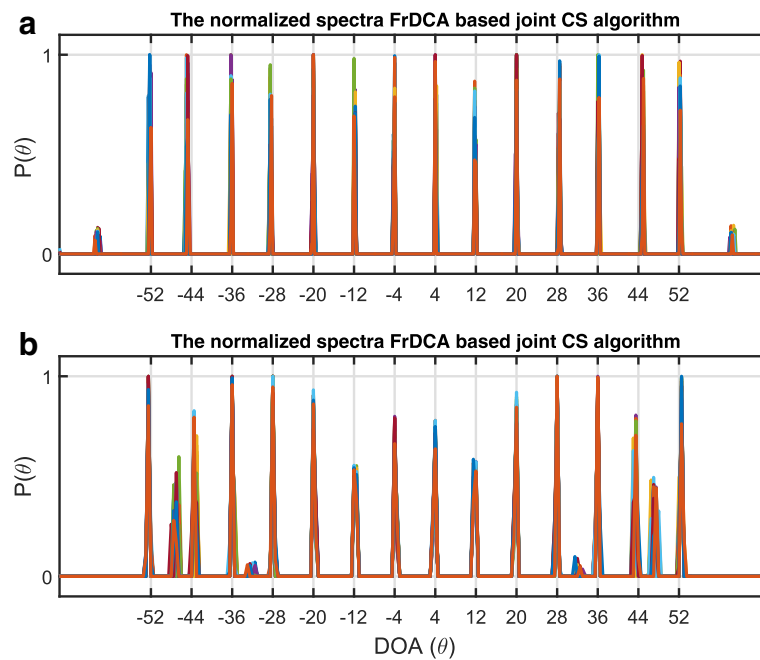
Page 9 of 12
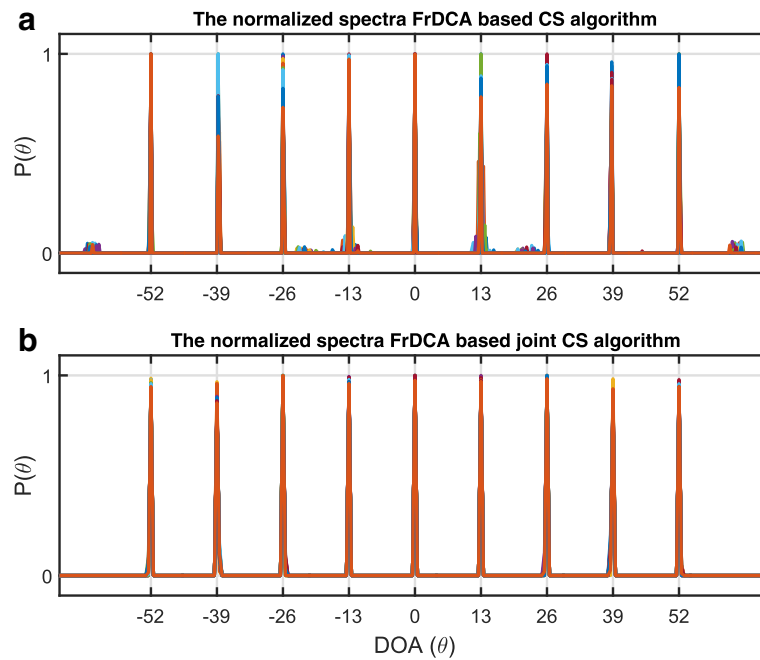
Fig. 5 The normalized spectra of two algorithms: **a** the FrDCA-based CS and **b** the FrDCA-based joint CS by using a six-element NLA from an environment containing nine wideband signals

relatively outperforms the CS model because the former takes the signal power fluctuation into full consideration. There are some low-level background noise, as shown in the spectra of CS algorithm, which are mainly generated by the power approximation.

In the fourth experiment, increase the number of sources to 14. The normalized spectra of 30 independent trials are illustrated in Fig. 6. It shows that the performance of FrDCA-based joint CS algorithm is greatly reduced. Many false peaks are presented in the spectra

Fig. 6 The normalized spectra of two algorithms: **a** the FrDCA-based CS **b** the FrDCA-based joint CS by using six-element NLA from environment containing 14 wideband signals

Liu *et al. EURASIP Journal on Advances in Signal Processing* (2016) 2016:133

Page 10 of 12

because the joint CS model does not possess enough DOF capacity to resolve so many sources. However, the CS algorithm can still maintain a good performance due to the increased DOF capacity.

4.3 RMSE

In this section, the performance of DOA estimation is compared via Monte Carlo trials. Hence, we define the average root-mean-square error (RMSE) of the estimated DOAs from 100 Monte Carlo trials as:

$$\text{RMSE} = \sqrt{\frac{1}{100D} \sum_{n=1}^{100} \sum_{k=1}^{D} \left(\tilde{\theta}_k(n) - \theta_k\right)^2} \tag{32}$$

where $\tilde{\theta}_k(n)$ is the estimation of θ_k for the nth trial. We compare how the SNR affects the DOA estimation.

The performances of four kinds of algorithms as a function of the input SNR or the number of snapshots are quantified by the RMSE of 100 independent trials in the aforementioned two simulation conditions ($D = 9, 14$). The other parameters are set as they are before. The RMSEs corresponding to different SNR for four kinds of algorithms are illustrated in Figs. 7 and 8, respectively. It is observed that three kinds of FrDCA-based algorithms generally outperform the auto-focusing-based MUSIC algorithm in all the conditions. The FrDCA-based joint CS algorithm achieves the best performance when the number of impinging source is 9, while its performance is reduced when the number of impinging source is increased to 14. The FrDCA-based MUSIC and CS algorithm is efficient and robust for the multi-source condition, especially when SNR $\geq$ 0 dB. However, their performances are greatly reduced when SNR $<$ 0 dB.
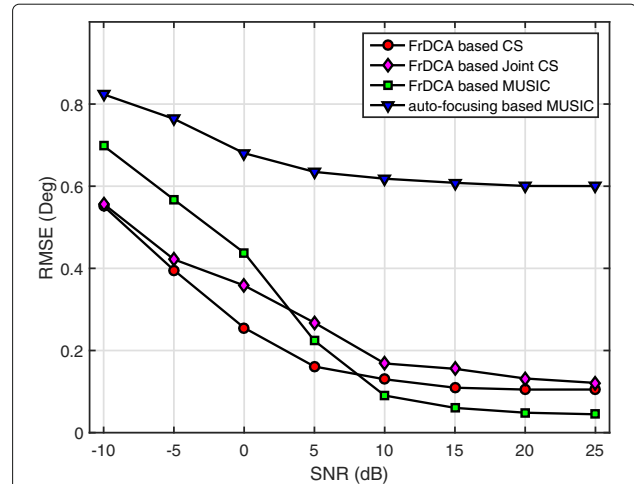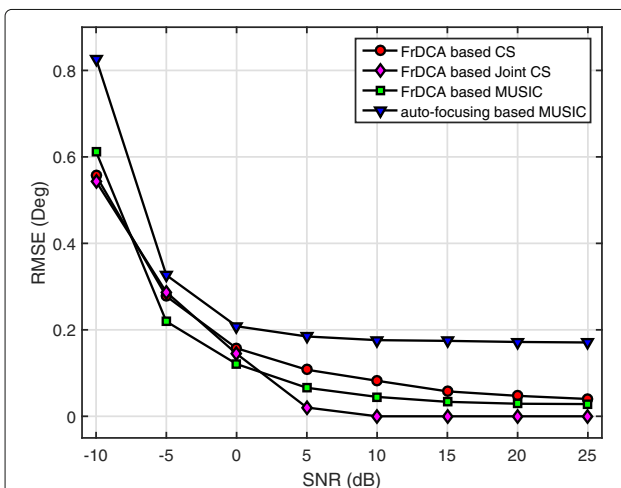

Fig. 8 The comparison of RMSEs corresponding to different SNR for four kinds of algorithms by using six-element array from an environment containing 14 wideband signals

The RMSEs corresponding to different number of snapshots are illustrated in Fig. 9. It is observed that the proposed FrDCA-based algorithms have already established a clear superiority. As the number of snapshots decreased, the signal power (variance matrix) estimation error are accordingly increased. Such estimation errors, which could be viewed as power fluctuation, would be spread in the FrDCA-based CS/MUSIC model. Therefore, their performance are greatly reduced in small number of snapshots compared to the joint CS algorithm.

4.4 The case of power fluctuation

In this section, we focus on the case of power fluctuation; assume that 9 LFM sources with 2-MHz bandwidth

Fig. 7 The comparison of RMSEs corresponding to different SNR for four kinds of algorithms by using six-element array from an environment containing nine wideband signals
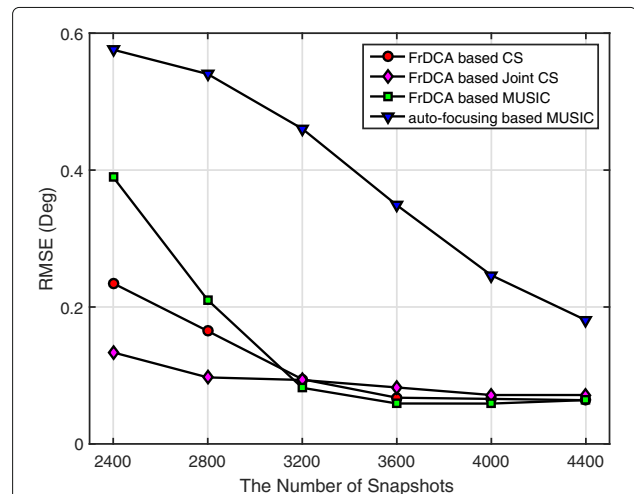

Fig. 9 The comparison of RMSEs corresponding to different number of snapshots for four kinds of algorithms by using six-element array from an environment containing 14 wideband signals

Liu *et al. EURASIP Journal on Advances in Signal Processing* (2016) 2016:133

Page 11 of 12

and f_{c_k} MHz center frequency are uniformly distributed in space from $-52°$ to $52°$, where $f_{c_k} = \{16, 17, 18, \cdots, 24\}$. In this setting, the signal power is significantly fluctuant and the FrDAC-based CS and MUSIC algorithms fail to work. We test the FrDCA-based joint CS algorithms by dividing the wideband signal into nine sub-bands based on the following parameter: $f_k = \{16, 17, \cdots, 24\}$ MHz, $f_0 = 20$ MHz, the bandwidth of all the sub-bands is 1 MHz. The normalized spectra of 30 independent trials are illustrated in Fig. 10. It shows that the joint CS algorithm can successfully resolve all sources in such a case of power fluctuation. The sharp peaks in the spectra indicate that the effectiveness of the algorithm and the measurement accuracy and precision are favorable.

5   Conclusions

Following the DCA perspective, we propose a FrDCA perspective by vectorizing structured SOS matrices. In a sense, it can be viewed as an extended structured model to generate virtual sensors including not only the conventional virtual sensors but also fractional ones. In practice, three DOA estimation algorithms for wideband signal based on proposed FrDCA are specifically presented. A wideband signal can be divided into several sub-band signals with different center frequencies. Then, by using FrDCA perspective, these sub-band signals can be further transformed into a group of virtual array signal with a fixed reference center frequency. In addition, by using the wideband signal to increase DOF capacity, more wideband sources than sensors (even more than virtual co-sensors) can be resolved. In the end, the corresponding numerical simulation results validate the advantages and the effectiveness of the proposed perspective through the performance comparisons with the existing algorithm.

Endnotes

[1] In the sequel, by analogy, $\mathbf{A}_{\mathbb{D}_i}(\mu_1 f, \theta)$ denotes the array manifold with the center frequency being $\mu_1 f$ and the array formulation being $\mathbb{D}_i$.

[2] To fully make use all the virtual sensors, a small number of correlation elements corresponding to the holes can be assigned with zero. In this setting, $\overline{\mathbb{U}} \nsubseteq \overline{\mathbb{D}}_1$ and the performance may be marginally improved.

Author details
[1]School of Information and Electronics, Beijing Institute of Technology, 5 South Zhongguancun Street, Haidian District, 100081 Beijing, People's Republic of China. [2]School of Electrical and Electronic Engineering, Nanyang Technological University, 50 Nanyang Avenue, Singapore, 639798, Singapore.

References
1. SH Talisa, KW O'Haver, TM Comberiate, MD Sharp, OF Somerlock, Benefits of digital phased array radars. Proc. IEEE. **104**(3), 530–543 (2016)
2. RO Schmidt, Multiple emitter location and signal parameter estimation. IEEE Trans. Antennas Propag. **34**(3), 276–280 (1986)
3. R Roy, T Kailath, Esprit-estimation of signal parameters via rotational invariance techniques. IEEE Trans. Acoust. Speech Signal Process. **37**(7), 984–995 (1989)
4. A Moffet, Minimum-redundancy linear arrays. IEEE Trans. Antennas Propag. **16**(2), 172–175 (1968)
5. E Vertatschitsch, S Haykin, Nonredundant arrays. Proc. IEEE. **74**(1), 217–217 (1986)
6. SU Pillai, Y Bar-Ness, F Haber, A new approach to array geometry for improved spatial spectrum estimation. Proc. IEEE. **73**(10), 1522–1524 (1985)
7. SU Pillai, F Haber, Statistical analysis of a high resolution spatial spectrum estimator utilizing an augmented covariance matrix. IEEE Trans. Acoust. Speech Signal Process. **35**(11), 1517–1523 (1987)
8. YI Abramovich, NK Spencer, AY Gorokhov, Detection-estimation of more uncorrelated Gaussian sources than sensors in nonuniform linear antenna arrays .l. fully augmentable arrays. IEEE Trans. Signal Process. **49**(5), 959–971 (2001)
9. J Li, P Stoica, *MIMO Radar Signal Processing*. (John Wiley and Sons Press, USA, 2009), pp. 365–410
10. P Pal, PP Vaidyanathan, Nested arrays: a novel approach to array processing with enhanced degrees of freedom. IEEE Trans. Signal Process. **58**(8), 4167–4181 (2010)
11. PP Vaidyanathan, P Pal, Sparse sensing with co-prime samplers and arrays. IEEE Trans. Signal Process. **59**(2), 573–586 (2011)
12. S Qin, YD Zhang, MG Amin, Generalized coprime array configurations for direction-of-arrival estimation. IEEE Trans. Signal Process. **63**(6), 1377–1390 (2015)
13. CL Liu, PP Vaidyanathan, Super nested arrays: linear sparse arrays with reduced mutual coupling-part i: Fundamentals. IEEE Trans. Signal Process. **64**(15), 3997–4012 (2016)
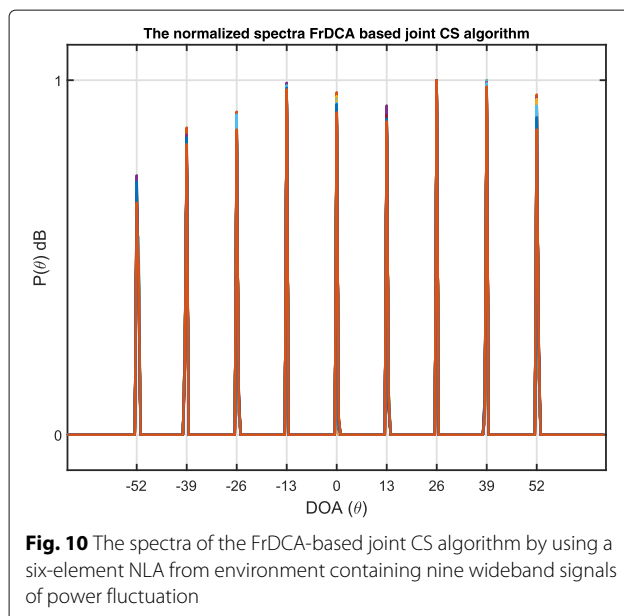

Fig. 10 The spectra of the FrDCA-based joint CS algorithm by using a six-element NLA from environment containing nine wideband signals of power fluctuation

Liu *et al. EURASIP Journal on Advances in Signal Processing* (2016) 2016:133

Page 12 of 12

14. CL Liu, PP Vaidyanathan, Super nested arrays: linear sparse arrays with reduced mutual coupling-part ii: High-order extensions. IEEE Trans. Signal Process. **64**(16), 4203–4217 (2016)

15. DD Ariananda, G Leus, Direction of arrival estimation for more correlated sources than active sensors. Signal Process. **93**(12), 3435–3448 (2013)

16. E BouDaher, Y Jia, F Ahmad, MG Amin, Multi-frequency co-prime arrays for high-resolution direction-of-arrival estimation. IEEE Trans. Signal Process. **63**(14), 3797–3808 (2015)

17. E BouDaher, F Ahmad, MG Amin, Sparse reconstruction for direction-of-arrival estimation using multi-frequency co-prime arrays. EURASIP J. Adv. Signal Process. **2014**(1), 1–11 (2014)

18. E BouDaher, F Ahmad, MG Amin, Sparsity-based direction finding of coherent and uncorrelated targets using active nonuniform arrays. IEEE Signal Process. Lett. **22**(10), 1628–1632 (2015)

19. D Romero, DD Ariananda, Z Tian, G Leus, Compressive covariance sensing: structure-based compressive sensing beyond sparsity. IEEE Signal Process. Mag. **33**(1), 78–93 (2016)

20. P Pal, PP Vaidyanathan, in *Signals, Systems and Computers, 2009 Conference Record of the Forty-Third Asilomar Conference on*. A novel autofocusing approach for estimating directions-of-arrival of wideband signals (IEEE, Pacific Grove, 2009), pp. 1663–1667

21. G Gelli, L Izzo, Minimum-redundancy linear arrays for cyclostationarity-based source location. IEEE Trans. Signal Process. **45**(10), 2605–2608 (1997)

22. MJ R, N Heinz, *Matrix Differential Calculus with Applications in Statistics and Econometrics*. (John Wiley and Sons Press, USA, 2007), pp. 31–35

23. R Tibshirani, Regression shrinkage and selection via the lasso. J. Roy. Statist. Soc. Ser. B Methodol. **58**(1), 267–288 (1996)

24. T-J Shan, M Wax, T Kailath, On spatial smoothing for direction-of-arrival estimation of coherent signals. IEEE Trans. Acoust. Speech Signal Process. **33**(4), 806–811 (1985)

25. C-L Liu, PP Vaidyanathan, Remarks on the spatial smoothing step in coarray music. IEEE Signal Process. Lett. **22**(9), 1438–1442 (2015)

26. Q Shen, W Liu, W Cui, S Wu, YD Zhang, MG Amin, Low-complexity direction-of-arrival estimation based on wideband co-prime arrays. IEEE/ACM Trans. Audio Speech Lang. Process. **23**(9), 1445–1456 (2015)

27. M Grant, S Boyd, CVX: Matlab Software for Disciplined Convex Programming, version 2.1 (2014). http://cvxr.com/cvx. Accessed 19 July 2016

28. M Grant, S Boyd, in *Recent Advances in Learning and Control. Lecture Notes in Control and Information Sciences*, ed. by V Blondel, S Boyd, and H Kimura. Graph implementations for nonsmooth convex programs (Springer London, London, 2008), pp. 95–110. http://stanford.edu/~boyd/graph_dcp.html